NASA TECHNICAL NOTE

NASA TN D-5687

c. 1

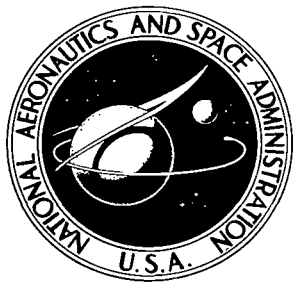

NASA TN D-5687

EFFECT OF WALL ROUGHNESS ON THE DAMPING OF LIQUID OSCILLATIONS IN RECTANGULAR TANKS

by Frank M. Bugg

George C. Marshall Space Flight Center
Marshall, Ala.

NATIONAL AERONAUTICS AND SPACE ADMINISTRATION • WASHINGTON, D. C. • MARCH 1970

1. REPORT NO.	2. GOVERNMENT ACCESSION NO.	3. RECIPI
NASA TN D-5687		

4. TITLE AND SUBTITLE

EFFECT OF WALL ROUGHNESS ON THE DAMPING OF LIQUID OSCILLATIONS IN RECTANGULAR TANKS

5. REPORT DATE: March 1970

6. PERFORMING ORGANIZATION CODE:

7. AUTHOR(S)

Frank M. Bugg

8. PERFORMING ORGANIZATION REPORT #: M159

9. PERFORMING ORGANIZATION NAME AND ADDRESS

George C. Marshall Space Flight Center
Marshall Space Flight Center, Alabama 35812

10. WORK UNIT NO.: 933-50-00-00-62

11. CONTRACT OR GRANT NO.:

12. SPONSORING AGENCY NAME AND ADDRESS

National Aeronautics and Space Administration
Washington, D.C. 20546

13. TYPE OF REPORT & PERIOD COVERED: Technical Note

14. SPONSORING AGENCY CODE:

15. SUPPLEMENTARY NOTES

This report was submitted as a thesis in partial fulfillment of the requirements for the degree of Master of Mechanical Engineering at the University of Virginia.

16. ABSTRACT

An experimental investigation was made to determine the effectiveness of wall roughness for damping liquid oscillations in rectangular tanks. Roughness with height equal to 0.427 percent of the wetted wall area gave damping 65 percent greater than the smooth wall damping. Comparisons were made with viscous damping theory.

EDITOR's NOTE: Use of trade names or names of manufacturers in this report does not constitute an official endorsement of such products or manufacturers, either expressed or implied, by NASA or any other U. S. agency.

17. KEY WORDS	18. DISTRIBUTION STATEMENT
	Unclassified - Unlimited

19. SECURITY CLASSIF. (of this report)	20. SECURITY CLASSIF. (of this page)	21. NO. OF PAGES	22. PRICE*
Unclassified	Unclassified	41	$3.00

*For sale by the Clearinghouse for Federal Scientific and Technical Information
Springfield, Virginia 22151

TABLE OF CONTENTS

LIST OF ILLUSTRATIONS

DEFINITION OF SYMBOLS

Symbol	Definition
a_n	Amplitude of nth cycle of liquid oscillation, cm
B	Tank width, cm
g	Acceleration in the direction tending to hold the liquid in the tank bottom, cm/sec^2
H	Distance of roughness strip from tank bottom, cm (Fig. 10)
h	Liquid depth, cm
k	π/L, 1/cm
L	Tank length, cm
n	Number of cycles
R	Reynolds number
S	Wetted perimeter at tank ends divided by twice the tank width
T	Temperature of test liquid, °F
V	Liquid velocity, cm/sec
w	Width of roughness strip, cm (Fig. 12)
δ	Log decrement of damping
ϵ	Roughness height, cm
ν	Kinematic viscosity of test liquid, cm^2/sec

DEFINITION OF SYMBOLS (Concluded)

Symbol	Definition
ρ	Liquid density, gm/cm^3
τ	Period of liquid oscillation, sec
μ	Liquid viscosity, gm/cm-sec
ω	Frequency of liquid oscillation, Hz
σ	Liquid surface tension, dynes/cm

EFFECT OF WALL ROUGHNESS ON THE DAMPING OF LIQUID OSCILLATIONS IN RECTANGULAR TANKS

SUMMARY

An experimental investigation was made to determine the effectiveness of wall roughness for damping liquid oscillations in rectangular tanks. The value of log decrement of damping (δ) increased in a nearly linear fashion as the roughness height was increased. With roughness whose height was 0.427 percent of the tank length covering 8.9 percent of the wetted wall area, δ was 65 percent greater than the smooth-wall value.

Roughness near the liquid surface was more effective in damping liquid oscillations than roughness deep in the tank with a sharp increase in δ corresponding to "wiping" of the roughness by the surface edge during decay. Maximum damping was produced by a particular roughness strip when the strip was at the maximum depth at which the surface edge wiped the roughness throughout decay of the oscillation. Narrow strips of roughness (3.6 percent of the wetted wall area) located in contact with the liquid surface edge during decay were found to produce 75 percent as much damping as roughness covering the entire end walls of the tank (36 percent of the wetted wall area).

The damping was found to increase with decreasing values of $L^{3/2}g^{1/2}/\nu$, a dimensionless viscosity parameter, but the increment of damping caused by wall roughness remained nearly constant through most of the $L^{3/2}g^{1/2}/\nu$ range. The increment of δ because of a particular wall roughness configuration was 34.5 percent of the total at $L^{3/2}g^{1/2}/\nu$ = 650 000 and was only 13.5 percent of the total δ at $L^{3/2}g^{1/2}/\nu$ = 27 000.

A formula was constructed to fit the smooth wall damping data through the range of values of $L^{3/2}g^{1/2}/\nu$ investigated by multiplying a theoretical equation for smooth wall viscous damping by an empirical constant. An expression formed by adding a term dependent on roughness height relative to tank length to the above formula gave a fair representation of the effect of roughness height on damping through a range of $L^{3/2}g^{1/2}/\nu$ values for a particular roughness configuration.

Reynolds number and boundary layer thickness calculations indicated that the test roughness should have little effect on viscous damping. Other calculations showed that the damping because of roughness could be produced by surface tension acting on the roughness-dependent wetted perimeter through a changing contact angle.

INTRODUCTION

Current space missions with their extensive use of liquid-fueled rockets have caused renewed interest in the dynamic behavior of contained liquids. A major portion of space vehicle mass may be propellant. As this liquid moves it exerts forces on the vehicle that will change the vehicle orientation if the forces are not counteracted by an attitude control system. A knowledge of the magnitude of forces exerted by the fuel, the frequency of fuel oscillations, and the amount of damping required to dissipate the oscillation energy is necessary for design of adequate and economical attitude control systems.

The external forces on a space vehicle may cause the acceleration environment affecting liquid motion to change by as much as 10 orders of magnitude during a particular mission (the primary source of external force might vary from rocket thrust to solar pressure). During the high acceleration boost phase of a typical flight, the propellant remains in the bottom of its tank, as expected, and moves primarily in its first slosh mode. The first mode is characterized by a rocking motion of the liquid surface with the maximum amplitudes occurring alternately at opposite sides of the tank. In Reference 1, Bauer calculated the natural mode shapes and frequencies for liquid oscillations which occur during boost, and analyzed a spring-mass model of the liquid system which can be used to determine forces on the tank walls. A similar spring-mass-damper model of the sloshing liquid is used by the National Aeronautics and Space Administration, along with the bending characteristics of the rocket, control system characteristics, and probable wind conditions at launch, to determine the stability of each vehicle in flight. In Reference 2 the first mode sloshing frequencies determined by a method similar to Bauer's were found to be in good agreement with measured values during the boost phase of a particular rocket flight. Flight data and drop tower tests (References 2 and 3, respectively) have shown that, for a wide range of tank sizes and liquid properties, the liquid remains in the container bottom moving primarily in its first mode, even though the acceleration tending to hold it there is on the order of 10^{-5} times that caused by the earth's

gravity. Frequencies predicted for the first mode in Reference 2 were accurate for sloshing in this near "weightless" condition. (Periods of 300 to 330 seconds were measured for a particular set of conditions, and the predicted value was 315 seconds.)

The effort to find effective ways of damping this first mode oscillation and to determine the damping available in particular fuel tanks has been almost entirely experimental and has included many kinds of damping devices (partitioned tanks, baffles, screens, floating cans, etc.). References 4 through 10 are examples of these experimental damping studies. As a result of such studies, ring baffles attached to the inside of the tank wall are used in many current launch vehicles to reduce liquid oscillations.

The purpose of the present investigation is to study another source of damping; that is, wall roughness of propellant tanks. Increasing the wall skin friction would be expected to increase the rate of damping of the first slosh mode. Some observations reported in Reference 11, a study of damping in smooth-wall tanks, tend to confirm this, indicating that even roughness of small height relative to the boundary layer thickness can produce damping three times as great as that for the smooth-wall case. References 12 and 13 suggest that surface tension affects damping. If surface tension affects damping, then a rough wall with its greater wetted perimeter should give greater surface-tension-related damping than a smooth wall. If wall roughness can provide adequate damping for some situations, there could be a savings in weight or manufacturing costs as compared with other damping devices, since the roughness might be sprayed on the tank interior or result during the forming of the tank. A literature search has revealed no studies of the effect of wall roughness on damping of liquid oscillations, although there are studies [11,12, 13] of damping because of smooth walls. The rate of damping was calculated in Reference 12 for sloshing in cylindrical tanks using laminar boundary layer theory and assuming that the different normal modes of sloshing were damped independently. In Reference 12 it was found that the experimental values for damping rate were from two to nine times as great as the values calculated for dissipation in a laminar boundary layer. Other factors suggested as possibly having an effect on damping were surface tension, wall roughness, boundary layer thickness, and interchange of energy between different slosh modes.

Reference 11 also used the laminar boundary layer theory to predict smooth-wall damping in cylindrical tanks. It is reported in Reference 11 that the measured damping was three times as great as predicted, before the test tanks were polished to mirror smoothness, and it is concluded that a

small amount of wall roughness greatly increased the damping. After the brass cylinders used in the investigation were polished to a mirror finish, experimentally determined values for log decrement were in good agreement with the theoretically determined values (calculated values were 2 to 7 percent higher than experimental values).

Keulegan [13] used the laminar boundary layer theory in conjunction with empirical results to formulate an expression for the log decrement of damping for a liquid sloshing in a smooth-wall rectangular tank. His experimental damping values were from 15 to 70 percent greater than those attributed to dissipation of energy in the boundary layer. The data of Reference 13 indicate that in large tanks the percentage of the damping occurring in the boundary layer is greater than in small tanks.

To accomplish the present investigation, tests were conducted in two rectangular glass tanks using silicon carbide grit bonded to the tank walls to produce roughness. The following specific objectives were set:

1. To determine the change in damping because of changes in roughness grain size (height).

2. To determine the effect on damping of changes in roughness location; that is, vary the depth of the roughness below the liquid surface and vary the portion of the wetted wall that is roughened.

3. To determine the effect of roughness height through a range of values of the dimensionless parameter $L^{3/2}g^{1/2}/\nu$.

4. To compare the experimental results of this investigation with the viscous damping predicted theoretically for the smooth-wall tank, and to empirically modify the theoretical damping expression so that it can be used to calculate the damping in the smooth-and rough-wall configurations of this investigation.

APPARATUS AND PROCEDURE

The small tank with pressure probes clamped in place on the tank ends is shown in the test setup (Fig. 1). The instruments shown are a 0.5-psi inductance-type differential pressure gage, a Carrier-type 1-127 amplifier and a Honeywell visicorder. The two glass tanks were commercial

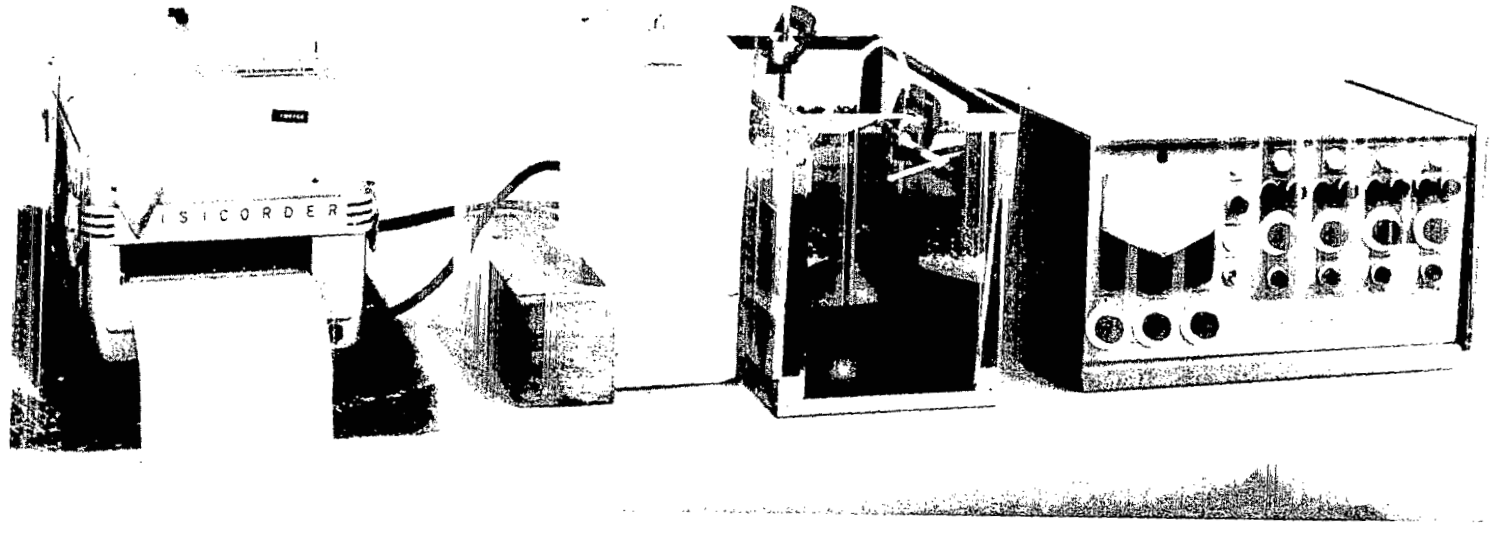

Figure 1. Test setup.

aquariums with inside dimensions as shown in Figure 2. Also shown in Figure 2 are the pressure probe locations and liquid levels used in the two tanks. The pressure probes, 14.6 cm in length, were of 0.64-cm steel tubing, with streamlined tips. They were mounted in wood blocks and clamped so that they were positioned 0.64 cm from the walls. The probes were connected to the gage by equal lengths of neoprene tubing.

The test liquids were distilled water plus aerosol MA (a wetting agent) and distilled water plus sucrose. The viscosity and density of the water-sucrose solutions were taken from tables in Reference 14. The surface tension of the aerosol MA-water solution was taken from Reference 13. The surface tension of the sucrose-water solutions was measured with a surface tension balance, and the viscosity of the aerosol MA-water solution was measured with an Oswalt-type viscometer by personnel of the Astronautics Laboratory of Marshall Space Flight Center. No difference was found between the viscosities of the aerosol MA-water solution and distilled water in the temperature range of interest. The kinematic viscosities of the test liquids are presented in Figure 3 as a function of temperature, and the surface tensions are shown in Figure 4.

Silicon carbide grit was applied to the tank walls to provide roughness. Figure 5 shows the dimensions of the five grit sizes used as measured using a magnifying glass and a scale. The area concentration for the different grit sizes is shown in Figure 6 and was determined by counting the number of particles per unit area. The average wetted perimeter at the tank ends was calculated from the grit dimensions and concentrations and was divided by twice the tank width to form parameter S (also presented in Figure 6). The wall area to be made rough was first outlined with masking tape and then covered with a thin film of rubber cement. The grit was sprinkled onto the rubber cement and pressed lightly against it. Because of this pressing of the particles against the walls, the minimum heights given in Figure 5 were thought to be more representative of roughness height than the maximum dimensions. Damping, which was measured with rubber cement alone on the tank walls, was found to be insignificantly higher than the smooth-wall damping (Table 1). The damping produced by the roughness (grit bonded to walls by rubber cement) was therefore considered to be due to the grit only.

To measure damping for a particular wall roughness configuration, the tank was first filled to the desired test level. The pressure probes were then clamped in place on the inside of the end tank walls and set at the proper depth. The amplifier was electrically balanced; a static calibration was made by placing one probe 1 inch deeper than the other and recording the output.

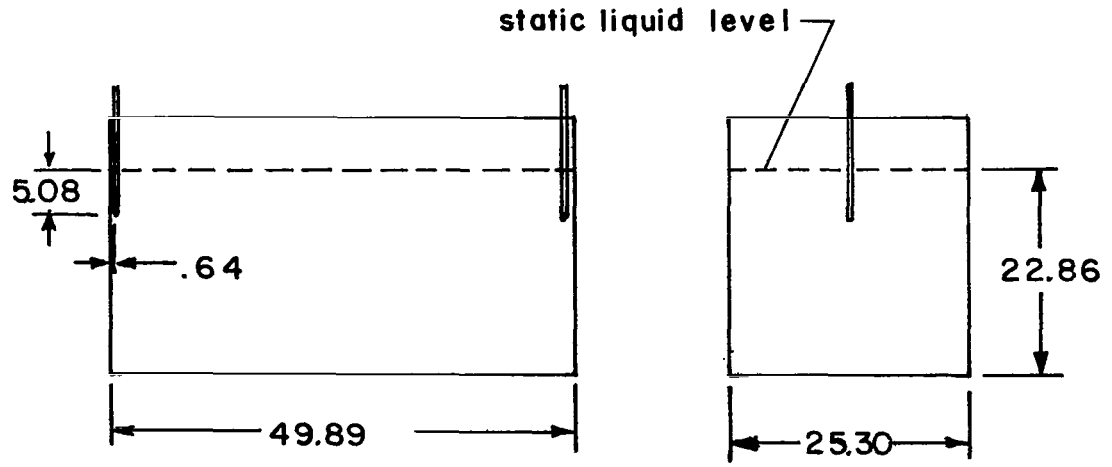

Large Tank

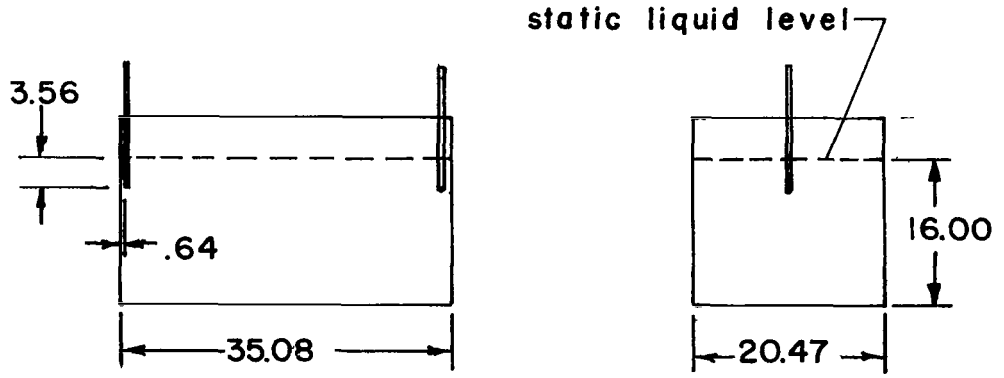

Small Tank

(All dimensions are in cm)

Figure 2. Tank dimensions.

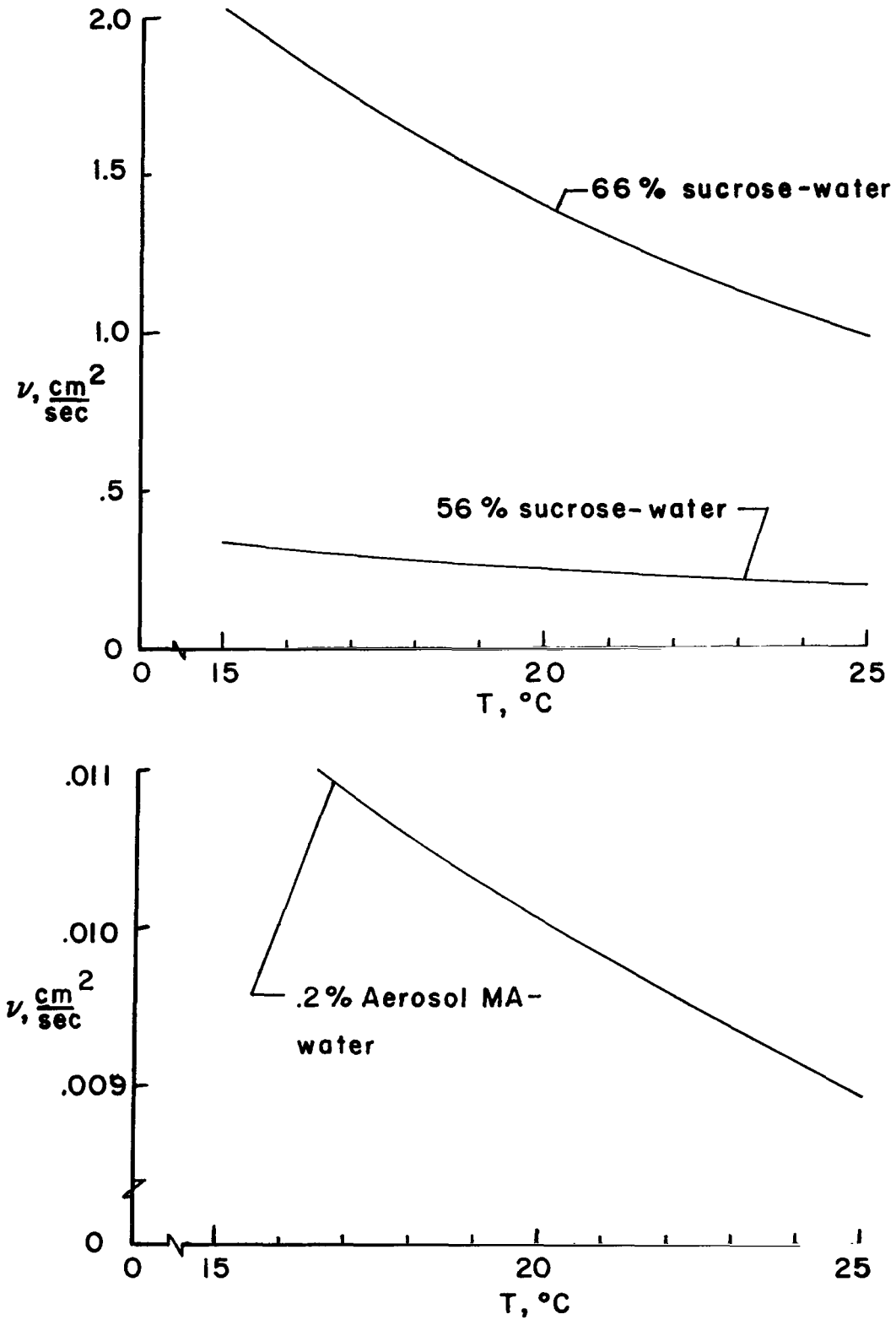

Figure 3. Test liquid kinematic viscosity.

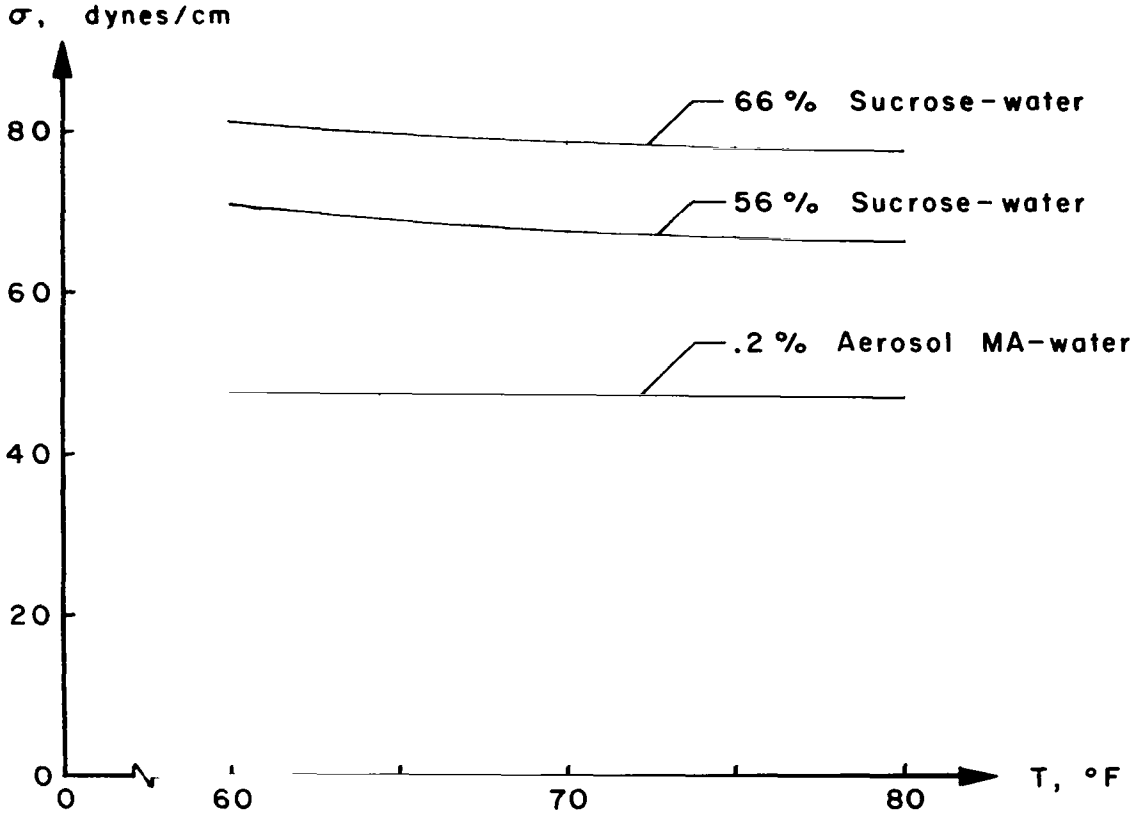

Figure 4. Test liquid surface tension.

The temperature of the test liquid was measured and recorded. With the test tank on a heavy steel table, a large amplitude (approximately 50 lb) periodic force was applied to the table at a frequency near the first mode frequency of the liquid. This force produced a small displacement (approximately 0.3 cm) of the table and gradually excited the first mode of liquid oscillation. When the liquid amplitude reached the desired height, the forcing was stopped and the amplitude was allowed to decay while the pressure differential between the probe tips was recorded. For each roughness condition, six decays were recorded, and after the sixth decay another static calibration was made and compared with the prerun calibration. The portion of the pressure record corresponding to decay from 1.27-cm liquid amplitude to 0.64-cm liquid amplitude was used to calculate the log decrement of damping for the large tank, and the portion corresponding to decay from 0.89- to 0.44-cm amplitude was used to determine the log decrement for the small tank.

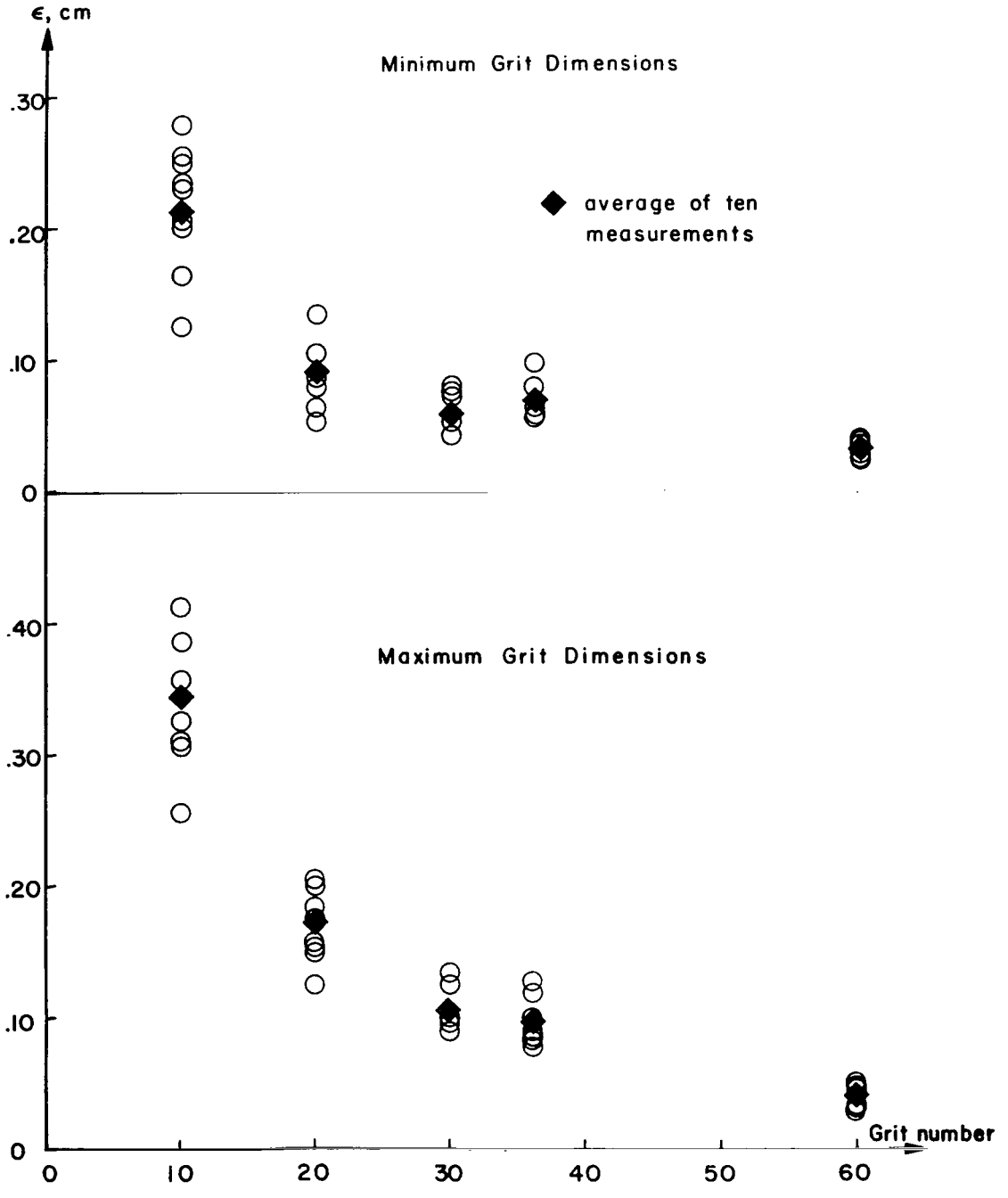

Figure 5. Roughness height.

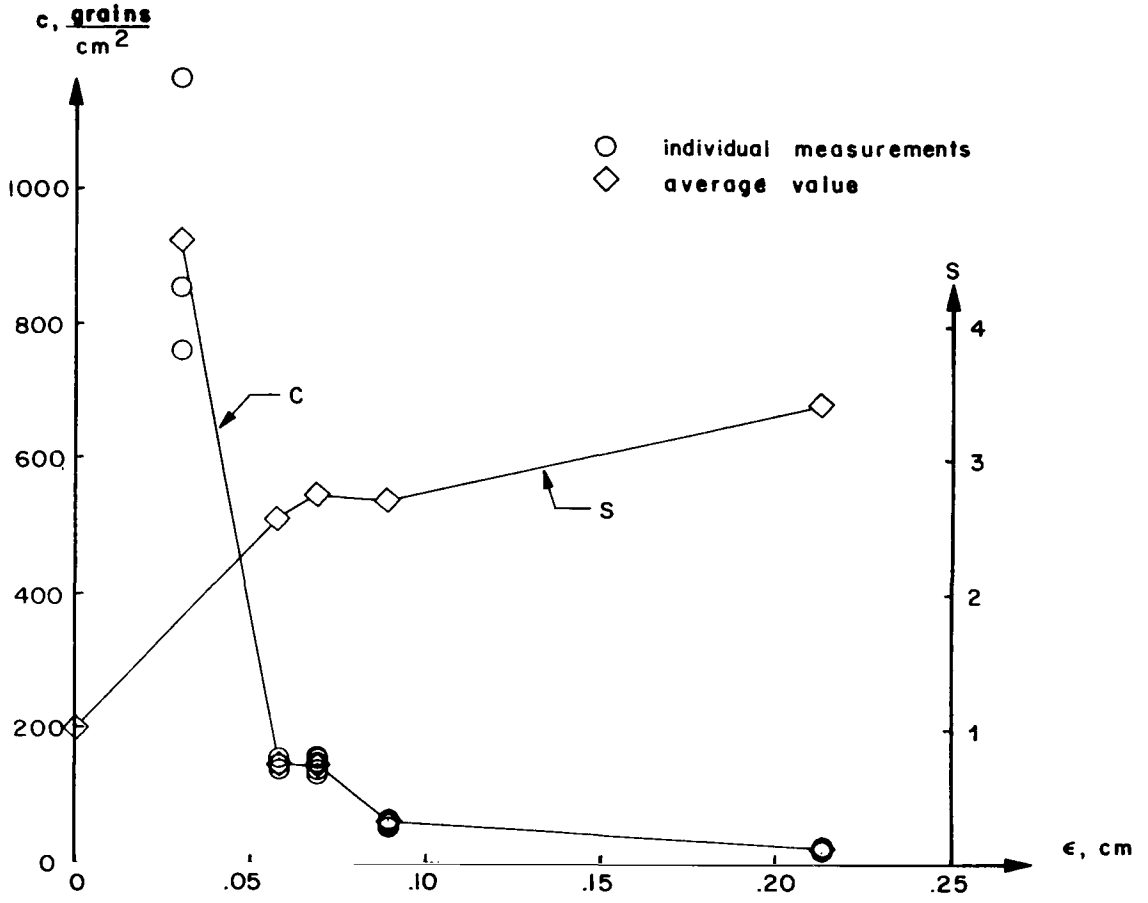

Figure 6. Grit distribution density and wetted perimeter.

The liquid oscillation frequency and damping were measured with the table free during decay and with the table immobile. No effect of table motion was found, and the majority of data were taken with the table free. The first mode oscillation was initiated as previously described in all cases except those in which the two most viscous test solutions were used, and for these the test tank was tilted to excite oscillations.

The frequency was measured by using timing marks on the decay record and by using a watch and counting cycles. A dynamic calibration was made by marking the record at points corresponding to observed liquid amplitudes at the tank walls. The phase relationship between the maximum liquid displacement amplitude and maximum pressure differential was

TABLE 1. EXPERIMENTAL RESULTS

Figure	L (cm)	H (cm)	w (cm)	ϵ (cm)	$2\epsilon/L$	Liquid	T (°C)	ν (cm^2/sec)	h (cm)	δ	ω (Hz)	R x 10^{-6}
-	49.9	17.8	7.6	Rubber cement	-	0.2% aerosol MA-water	22.2	0.0095	22.9	0.0151	1.24	1.17
8		-	-	0	0		25.6	0.0087		0.0146		1.28
		17.8	7.6	0.213	0.0086		22.2	0.0095		0.0241		1.17
				0.089	0.0036		23.9	0.0091		0.0194		1.22
				0.069	0.0028		20.0	0.0100		0.0187		1.11
				0.058	0.0023		24.4	0.0090		0.0179		1.23
				0.030	0.0012		19.4	0.0101		0.016		1.10
10		0		0.213	0.0086		21.7	0.0096		0.0152		1.16
		5.1					20.0	0.0100		0.0156		1.11
		10.2					20.6	0.0098		0.0164		1.13
		12.7					22.2	0.0095		0.0171		1.17
		14.0					20.6	0.0098		0.0177	1.25	1.13
		15.2					22.8	0.0093		0.0204	1.24	1.19
		16.5					21.6	0.0096		0.0249		1.16
		17.8					22.2	0.0095		0.0241		1.17
		19.1					18.3	0.0104		0.0240		1.07
		21.6					20.0	0.0100		0.0226	1.25	1.11
		22.9								0.0190	1.24	
12		-	0	-	-					0.0150		
		22.9	1.3	0.213	0.0086					0.0190		
		21.6	2.5							0.0226	1.25	
		19.1	5.1				18.3	0.0104		0.0240	1.24	1.07
		17.8	6.4				20.0	0.0100		0.0187		1.11
		16.5	7.6				21.6	0.0096		0.0249		1.10
		15.2	8.9				18.3	0.0104		0.0242		1.07
		7.6	16.5				20.0	0.0100		0.0250		1.11
		0	24.1				19.4	0.0101		0.0253		1.10
13	35.1	-	-	0	0	66% sucrose-water	18.8	1.48	16.0	0.222	1.44	0.00440
		12.4	5.3	0.089	0.0051		21.1	1.29		0.206	1.44	0.00507
				0.213	0.012		21.1	1.29		0.197	1.46	0.00507
		-	-	0	0		23.4	1.09		0.185	1.46	0.00593
		12.4	5.3	0.058	0.0033		21.6	1.22		0.191	1.45	0.00531
				0.089	0.0051		22.2	1.20		0.191	1.48	0.00545
				0.213	0.012		22.8	1.11		0.180	1.46	0.00586
		-	-	0	0	56% sucrose-water	18.8	0.268		0.0881		0.0242
		12.4	5.3	0.058	0.0033		22.8	0.218		0.0843		0.0299
				0.089	0.0051		21.1	0.241		0.0888		0.0270
				0.213	0.012		20.0	0.254		0.0987	1.47	0.0256
		-	-	0	0	0.2% aerosol MA-water	19.4	0.0101		0.019	1.40	0.642
		12.4	5.3	0.058	0.0033		20.6	0.0098		0.021	1.42	0.662
				0.089	0.0051		20.6	0.0098		0.023		0.662
				0.213	0.012		20.0	0.0100		0.029		0.650

investigated by marking the pressure decay record when maximum liquid amplitude was observed for several cycles.

A flow visualization exercise was performed. The motion of small, nearly neutrally buoyant particles was observed at various depths in the small tank during the first mode liquid oscillation.

DISCUSSION

Throughout the discussion the damping is represented by the log decrement of damping (δ) where

$$\delta = \frac{1}{n} \ln \frac{a_o}{a_n} .$$

Liquid oscillation amplitudes of 1.27 and 0.64 cm were used as a_o and a_n, respectively, for data taken in the large tank. For data from the small tank, 0.89 and 0.44 cm were used for a_o and a_n, respectively; n is the number of cycles between a_o and a_n. A line was faired through the peaks of the pressure decay record and the pressure differentials corresponding to a_o and a_n were marked as shown in Figure 7 on a typical pressure decay record. The number of cycles between these marks was counted and used for the value of n in the equation above; δ was independent of amplitude for the range of amplitudes investigated.

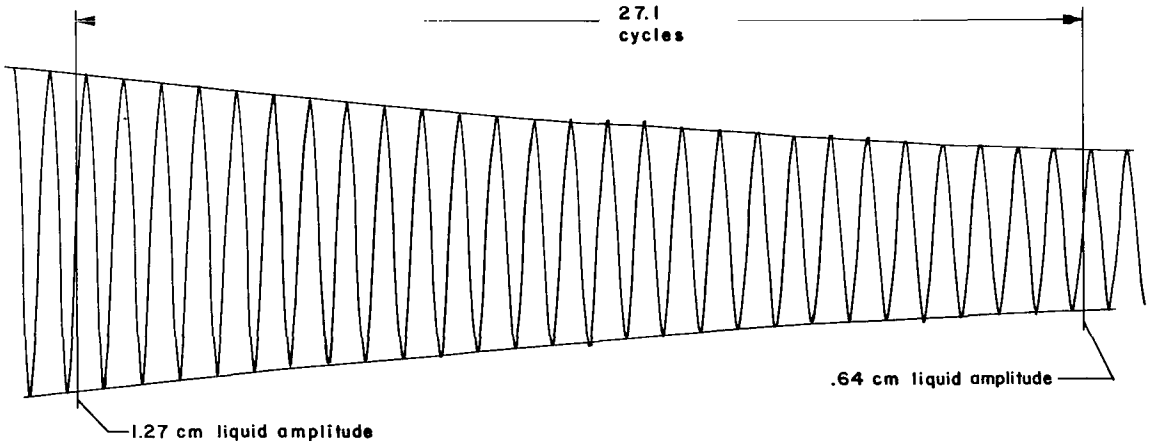

Figure 7. Typical pressure differential decay record.

During decay of the liquid oscillation, the liquid surface was smooth (except as noted later) with no splashing or frothing. This orderly first mode oscillation characterized by a rocking motion of the liquid surface is the situation of interest as described in the introduction. Bubbles that formed on the tank wall were removed before data were taken since they were generally of the same height as the test roughness. Bubbles that were trapped in the high viscosity sucrose-water solutions during the mixing of the solutions were removed before data were taken so that they would not affect the liquid properties.

The variables considered to have affected the damping of free oscillations in smooth-wall rectangular basins for this investigation were ρ, μ, g, L and B. The tank depth is not an important variable if the ratio of depth to length is approximately 0.5 or greater, as was the case [1]. The capillary forces were small compared to gravity forces (gravity/capillary = 4100) and the contact angle was, in the first part of this investigation, assumed to remain constant during the oscillations. Therefore, with this assumption, the surface tension was not considered to be a significant variable. Applying dimensional analysis to the five variables resulted in two dimensionless parameters, B/L and $L^{3/2}g^{1/2}\rho/\mu$. The latter or $L^{3/2}g^{1/2}/\nu$ is a useful parameter for comparing data from tanks in different acceleration environments and is thus sometimes used in the study of liquid dynamics in space vehicles. The dimensionless viscosity parameter ($L^{3/2}g^{1/2}/\nu$) has been called Reynolds number in some of the literature of liquid sloshing, probably because any characteristic velocity chosen for the purpose of calculating Reynolds number is a function of $g^{1/2}L^{1/2}$. If a fluid dynamic system existed in which the velocity was equal to $g^{1/2}L^{1/2}$, then the basic force ratios would become

$$\frac{\text{inertia}}{\text{viscous}} = \frac{VL\rho}{\mu} = \frac{L^{3/2}g^{1/2}}{\nu} ,$$

$$\frac{\text{inertia}}{\text{gravity}} = \frac{V^2}{Lg} = 1,$$

and

$$\frac{\text{inertia}}{\text{surface tension}} = \frac{V^2L\rho}{\sigma} = \frac{gL^2\rho}{\sigma} .$$

Some specific flight situations having values of $L^{3/2}g^{1/2}/\nu$ in the range covered by this study (though the tank shapes are different) are the S-IVB liquid hydrogen tank in low earth orbit ($L^{3/2}g^{1/2}/\nu = 86 \times 10^4$) and the Apollo service module propellant tanks in low earth orbit ($L^{3/2}g^{1/2}/\nu = 1.5 \times 10^4$). The S-IVB stage and the Apollo service module are the third and fourth stages, respectively, of the National Aeronautics and Space Administration's Saturn V launch vehicle, and their tank diameters, 260 inches and 52 inches, respectively, were used for the value of L above. The sucrose-water solutions were chosen as test liquids because they provided a simple and accurate method of obtaining a broad range of values of $L^{3/2}g^{1/2}/\nu$, and the aerosol MA-water solution was chosen instead of pure water for the high $L^{3/2}g^{1/2}/\nu$ values to avoid problems associated with use of pure water as reported by other investigators [8, 13]. Slight contamination of the test tank walls and liquid surface was reported to have a large effect on damping when water was the test solution, but use of water plus a wetting agent or other detergent-like test liquids alleviated this problem. The results of this investigation are directly applicable only to rectangular tanks of the shape used here, but should be sufficient for determining the feasibility of using wall roughness as a damping device in tanks of other shapes.

The data shown in the figures are also listed in Table 1. The average run was repeatable within 1.8 percent.

Effect of Roughness Height

Figure 8 shows the nearly linear increase in δ with roughness height. The largest value of δ shown is about 65 percent greater than the smooth-wall value, and this is with roughness covering 8.9 percent of the wetted wall area. The bars through data points in this figure show the spread of data, and the symbols are the average of six values measured for each roughness condition. In succeeding figures, only the average values are presented. A least squares curve fit was used to determine the straight line through the data points.

Checks of these results were difficult because of lack of data for comparable configurations. The value shown for smooth-wall damping is about 50 percent higher than the value measured by Keulegan [13] in a smooth-wall rectangular basin of about the same width, but having a depth and length about 2.3 times as great.

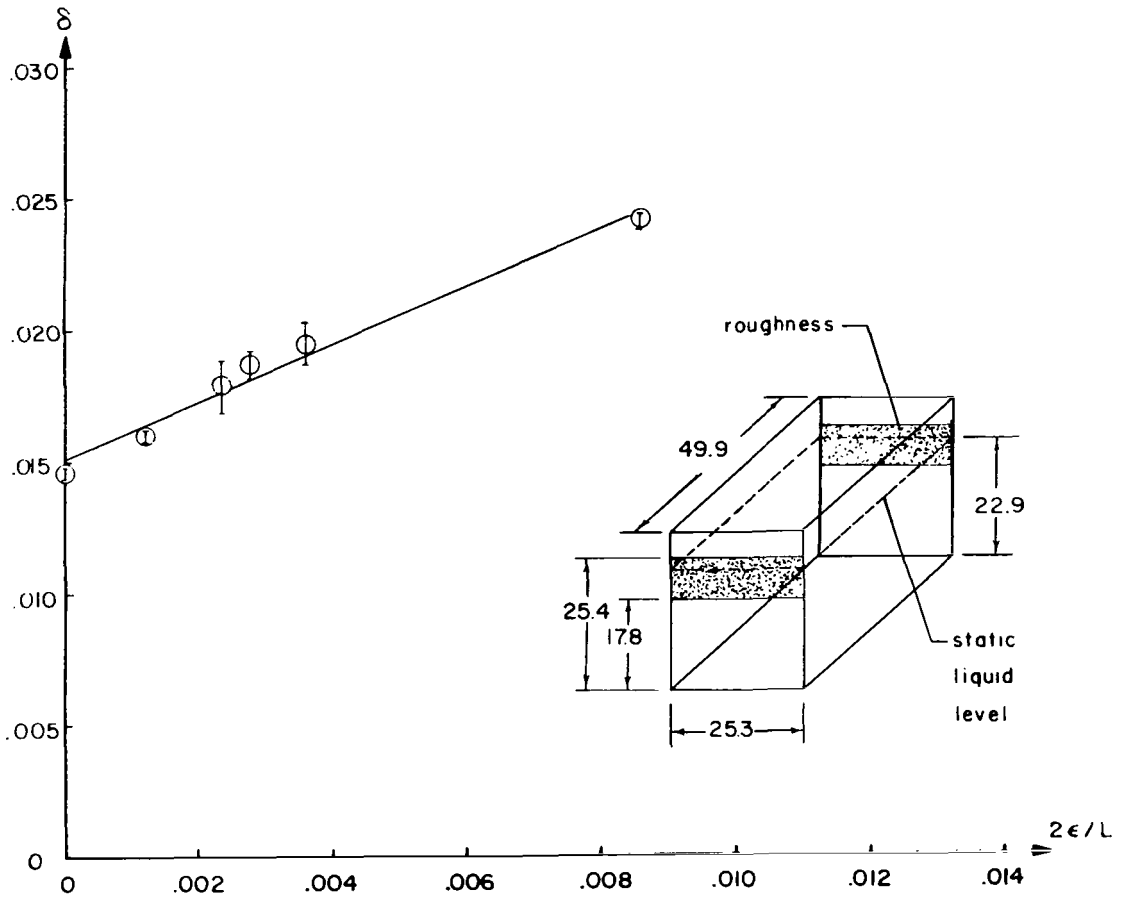

Figure 8. Effect of roughness height.

Effect of Roughness Location

In Reference 1, Bauer showed that for liquid sloshing in a cylindrical tank, essentially all of the motion takes place within one radius of the liquid surface and the liquid deep in the tank is nearly stationary. A similar situation was found in the rectangular tanks of the present investigation. The motion of small, nearly neutrally buoyant particles was observed in the small tank during the first mode oscillation. The results of the observation are sketched in Figure 9. A 3-cm peak-to-peak maximum amplitude produced approximately 3-cm travel of a particle at the surface node along the path shown, produced about a 0.3-cm movement of particles 3 cm from the bottom

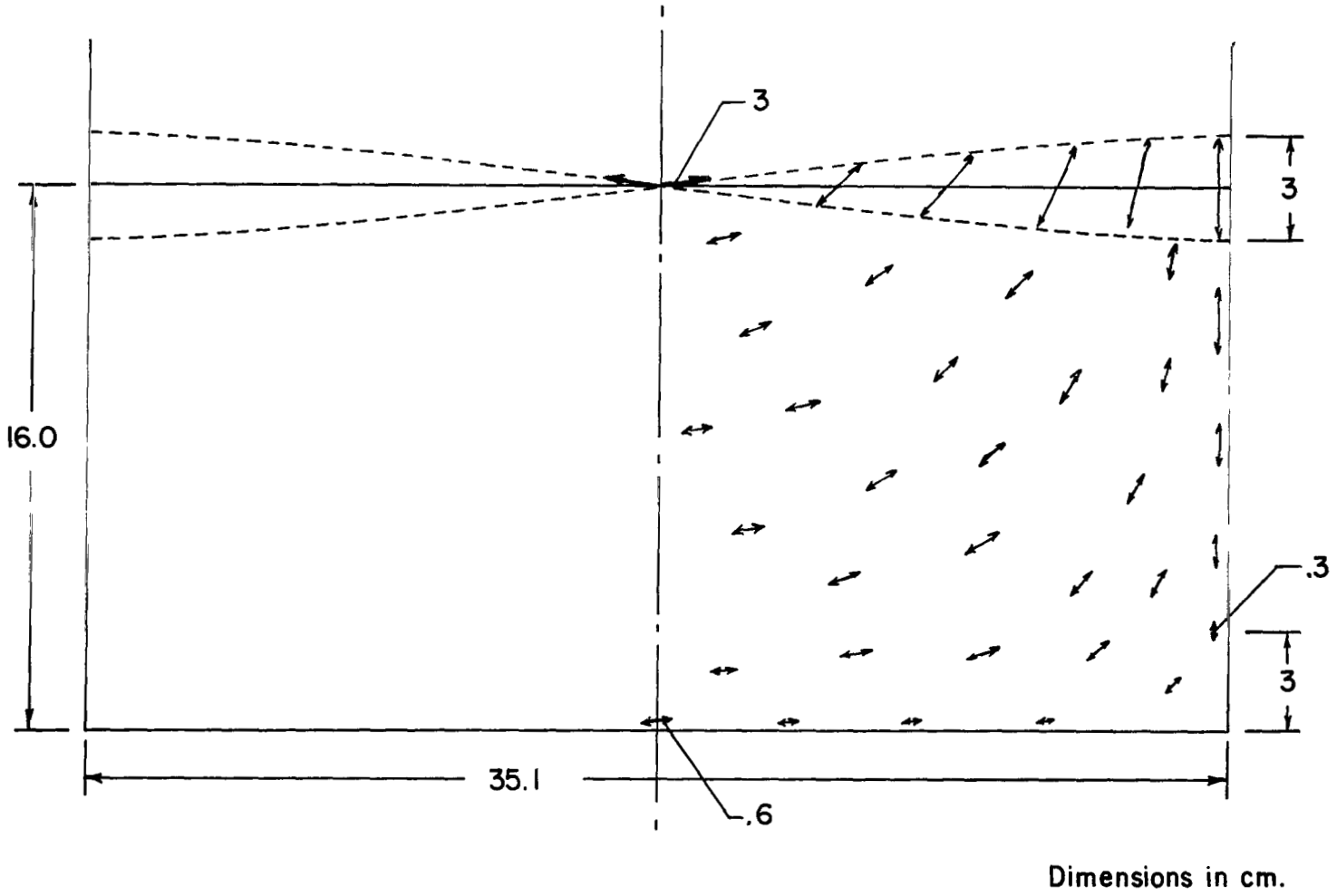

Figure 9. Flow pattern.

near the tank end, and gave a 0.6-cm travel of particles at the tank bottom center. The arrows give the approximate direction of motion, but not the magnitude.

Since the resistance to liquid motion provided by the roughness should increase with the liquid velocity at the roughness location, it was expected that the effectiveness of roughness for damping the oscillations would increase as it was moved from deep in the tank to the liquid surface. The data of Figure 10 show the expected result. As the roughness was moved from the low-velocity region at the tank bottom to the maximum velocity at the surface, the value of δ increased from near the value for the smooth-walled configuration to about 1.7 times the smooth-wall value.

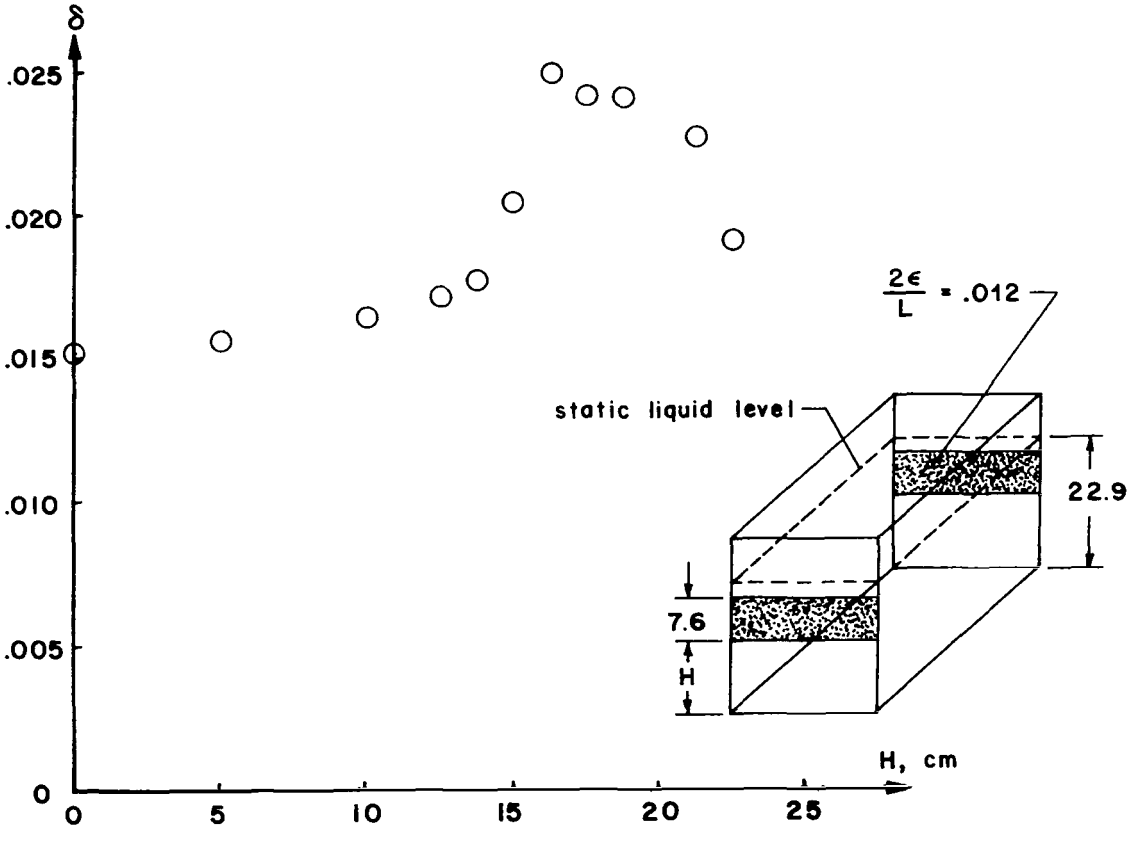

Figure 10. Effect of roughness depth.

At H = 14.0 cm, the upper edge of the roughness touched the liquid surface edge when the amplitude was 1.27 cm. Therefore, the sharp increase in δ as H was increased above 14.0 cm corresponded to the surface edge wiping the roughness during a portion of the decay. The maximum value of damping occurred at H = 16.5 cm, the smallest value of H for which the roughness is wiped by the liquid surface edge at each end of the tank during the entire decay from 1.27- to 0.64-cm amplitude. The largest value of H for which the roughness is wiped by the liquid surface throughout decay is H = 21.6 cm. It is seen that δ decreases sharply as the roughness is moved higher. Figure 11 shows the liquid oscillating in its first mode with the liquid edge wiping smooth walls in (a) and wiping the roughness strips on the tank ends in (b). The ripples on the surface in (b) represent part of the energy that has been removed from the first mode oscillation by the roughness strips as they break the liquid surface edge. These ripples were not present during sloshing with the roughness strip not in contact with the liquid surface.

The data of Figure 12 also indicate the effectiveness of roughness in contact with the liquid surface. Strips of roughness 2.54 cm wide located so that the liquid surface edge was wiping the grit throughout the decay produced approximately 75 percent as much damping as 24.13-cm wide strips reaching from the tank bottom to the highest liquid oscillation amplitude.

The surface damping effects are further discussed in The Discussion of Flow Regimes and the Mechanism of Damping Because of Roughness Section.

Effect Of Roughness At Various Values Of $L^{3/2}g^{1/2}/\nu$

The effect of roughness on δ through a range of values of $L^{3/2}g^{1/2}/\nu$ is shown in Figure 13. The roughness was located for nearly maximum effectiveness (that is, the liquid surface edge wiped the roughness throughout the decay). The open symbols are data taken using the small tank with the roughness configuration shown in the sketch. The solid symbols are data from the large tank and these were shown in Figure 8. The small tank was 70 percent as long as the large tank; this ratio of lengths was used to scale liquid depth, probe depth, amplitude, and roughness location. The small tank was 81 percent as wide as the large tank.

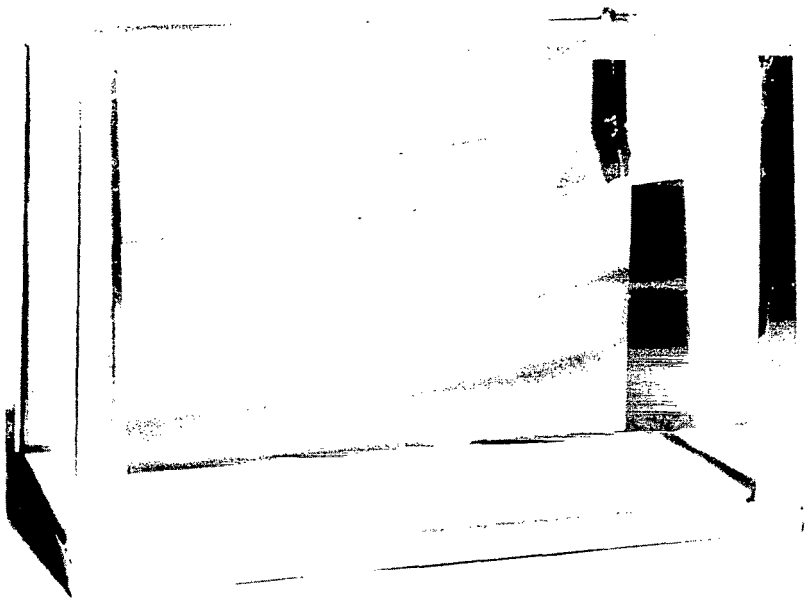

(a.) Smooth wall

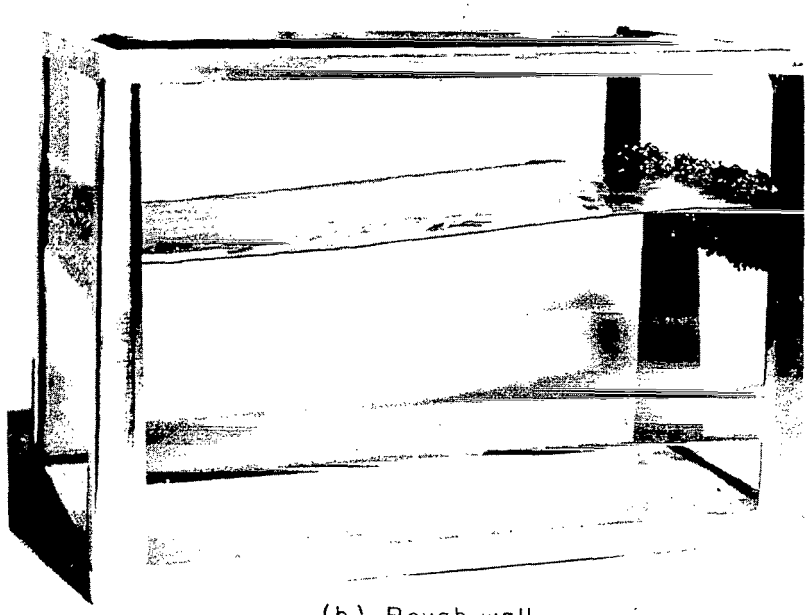

(b.) Rough wall

Figure 11. Effect of roughness on surface activity.

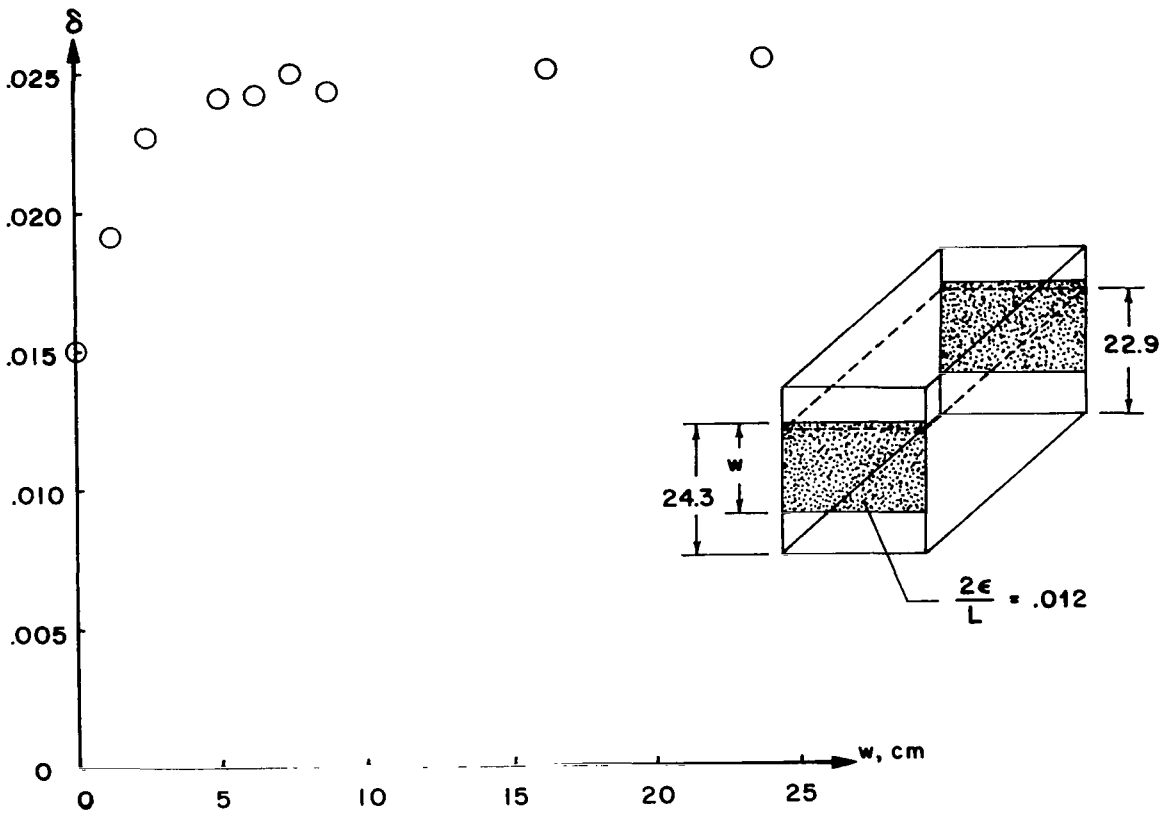

Figure 12. Effect of roughness strip width.

The change in $L^{3/2}g^{1/2}/\nu$ was produced primarily by using sucrose-water solutions of different viscosities as listed in Table 1. The change in $L^{3/2}g^{1/2}/\nu$ from about 650 000 to 1 200 000 was due to the change in tank size. The damping increased with decreasing values of $L^{3/2}g^{1/2}/\nu$.

In Reference 13, Keulegan used potential flow and boundary layer theory to derive an expression for damping caused by viscous action in a smooth-wall rectangular container:

$$\delta_\nu = \pi^{-1/2}\left[(\pi + Bk) + \frac{Bk(\pi - 2kh)}{\sinh 2kh} \right] \frac{\nu^{1/2}\ \tau^{1/2}}{B} + 2k^2\nu\tau. \qquad (1)$$

The first term on the right-hand side of equation (1) represents viscous damping in the boundary layer, and the second term represents viscous damping in the body of the fluid. Keulegan verified this equation by experiment.

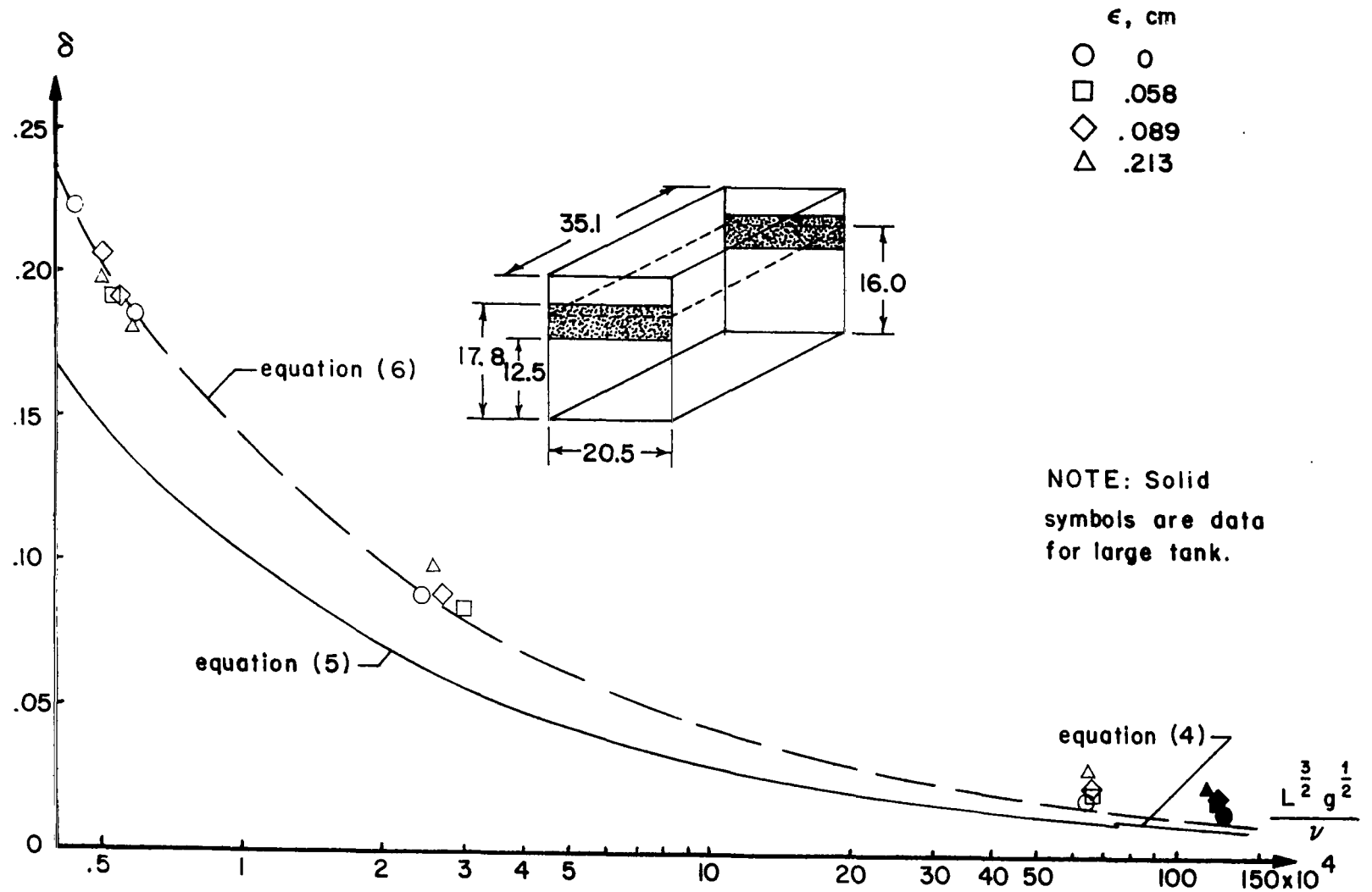

Figure 13. Effect of $L^{3/2}g^{1/2}/\nu$ and roughness height.

The damping predicted by this equation for his largest test tank, where surface effects were small compared to viscous effects, was in good agreement with the measured damping. His experimental results were for a range of tank sizes (23.8 to 242 cm in length), and the experimental damping values were approximately 15 to 70 percent higher in going from large to small tanks than the values caused by viscous losses as computed by equation (1). Keulegan concluded that the losses not caused by viscous action were primarily due to some type of surface activity and used experimental results to modify equation (1), bringing it closer to the measured damping. A similar procedure is used in the present investigation.

In Reference 13 the expression found for the square of the first mode frequency was:

$$\omega^2 = \frac{\pi g}{L} \tanh \frac{\pi h}{L} \quad . \tag{2}$$

The frequencies calculated for the tanks of the present investigation using equation (2) were 1.18 and 1.41 Hz for the large and small tanks respectively compared to measured values of 1.24 and 1.48 Hz. The calculated frequencies are below the actual values by less than 5 percent; this agreement is about the same as found in the literature for other comparisons of predicted and experimental sloshing frequencies.

Equations (1) and (2) were combined with the term $L^{3/2}g^{1/2}/\nu$ to obtain:

$$\delta_v = \left[(\pi + Bk) + \frac{Bk(\pi - 2kh)}{\sinh 2kh} \right] \frac{2^{1/2}\ \pi^{3/4}}{Bk(\tanh\ kh)^{1/4}} \ (\nu/L^{3/2}g^{1/2})^{1/2}$$

$$+ \frac{4\pi^{5/2}}{(\tanh\ kh)^{1/2}} \ (\nu/L^{3/2}g^{1/2}). \tag{3}$$

The dimensions and liquid depths for the large and small tanks were substituted into equation (3), and the following equations were obtained for viscous damping in the large and small tanks, respectively:

$$\delta_{v_L} = 10.3\ (\nu/L^{3/2}g^{1/2})^{1/2} + 74(\nu/L^{3/2}g^{1/2}) \quad (4)$$

$$\delta_{v_S} = 9.40\ (\nu/L^{3/2}g^{1/2})^{1/2} + 74.0\,(\nu/L^{3/2}g^{1/2}). \quad (5)$$

There are two equations because the tanks were not geometrically similar with regard to width. Curves are plotted from these equations in Figure 13 for comparison with the smooth-wall data (circular symbols). The tanks of the present investigation differ from the tanks in Reference 13 in length-to-width ratio, but have lengths in the range of lengths covered by Reference 13. The experimental smooth-wall damping values presented in Figure 13 are approximately 41 percent higher than the calculated values for viscous losses in the small tank and about 56 percent higher than those calculated for the large tank. These results appear reasonable when compared with the results of Reference 13.

Equation (5) was multiplied by an empirical factor, 1.41, as the first step in constructing a formula to represent experimental results for the small tank. Since the difference between equations (4) and (5) is small and because measurements were taken at essentially only one value of $L^{3/2}g^{1/2}/\nu$ for the large tank, only equation (5) was used. The result of multiplying equation (5) by 1.41 is:

$$\delta_S = 13.3(\nu/L^{3/2}g^{1/2})^{1/2} + 104(\nu/L^{3/2}g^{1/2}). \quad (6)$$

The dashed curve in Figure 13, calculated by equation (6), appears to give a good representation of smooth-wall damping (circular symbols).

To find the change in damping with roughness height at specific values of $L^{3/2}g^{1/2}/\nu$, the dashed curve in Figure 13 was used as a guide, and the differences between smooth- and rough-wall damping were taken from Figure 13 at four values of $L^{3/2}g^{1/2}/\nu$. These results are shown in Figure 14. The method of least squares was used to fit straight lines through the points at each value of $L^{3/2}g^{1/2}/\nu$ in Figure 14. The effect of roughness height seems to be about the same for the three largest values of $L^{3/2}g^{1/2}/\nu$ in Figure 14. A possible explanation of the loss of effectiveness of roughness at $L^{3/2}g^{1/2}/\nu$ = 5000 is presented in the next section. The slopes of these damping-versus-roughness-height curves do not show a consistent effect of $L^{3/2}g^{1/2}/\nu$.

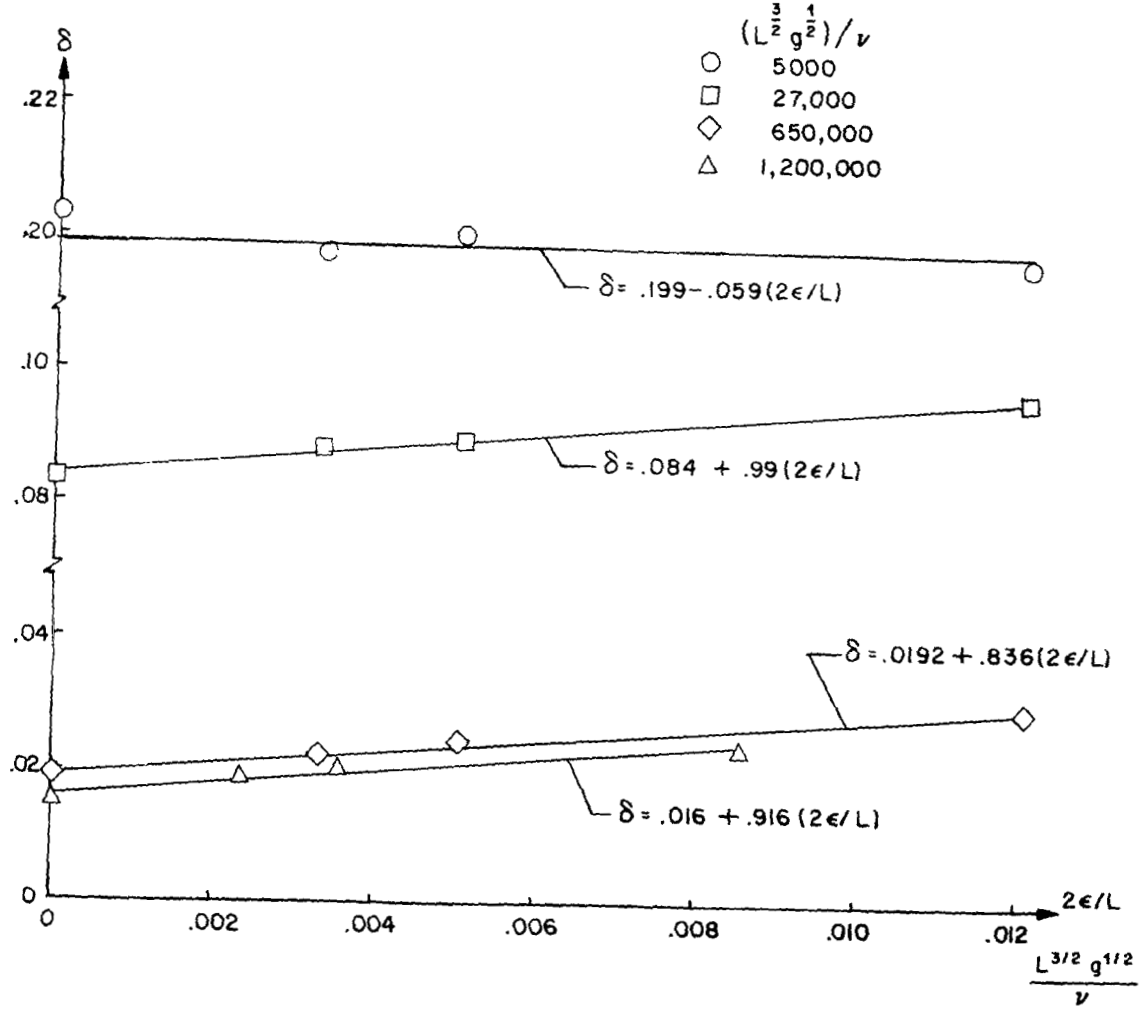

Figure 14. Effect of roughness height at particular values of $L^{3/2}g^{1/2}/\nu$.

The slopes of the three lower curves in Figure 14 were assumed to be representative of slopes in the $L^{3/2}g^{1/2}/\nu$ range 27 000 to 1 200 000. The product of the average of these three slopes and $2\epsilon/L$ was added to equation (6) as follows:

$$\delta = 13.3\,(\nu/L^{3/2}g^{1/2})^{1/2} + 104(\nu/L^{3/2}g^{1/2}) + 0.914(2\epsilon/L). \qquad (7)$$

Curves calculated using equation (7) are shown in Figure 15 with the data from Figure 13. These data and equation (7), constructed to fit these data, indicate that the increment of damping gained by having rough walls is nearly independent of $L^{3/2}g^{1/2}/\nu$ from $L^{3/2}g^{1/2}/\nu = 27\,000$ to $L^{3/2}g^{1/2}/\nu = 1\,200\,000$. The percentage of total damping because of wall roughness decreases, therefore, with decreasing values of $L^{3/2}g^{1/2}/\nu$. In application this means that use of wall roughness for damping would be more practical, for instance, in the S-IVB liquid hydrogen tank in low-earth orbit ($L^{3/2}g^{1/2}/\nu = 86 \times 10^4$) than in Apollo service module propellant tanks in low-earth orbit ($L^{3/2}g^{1/2}/\nu = 1.5 \times 10^4$).

Discussion of Flow Regimes and the Mechanism of Damping Because of Roughness

Reynolds number values were calculated for the oscillating fluid based on the maximum velocity at the liquid surface edge and the maximum amplitude at the tank wall at the start of each free decay. The damping is plotted as a function of this Reynolds number in Figure 16; the largest Reynolds number is seen to be about 1500. If the transition Reynolds number on a flat plate in a uniform constant-velocity flow ($R_{tran} = 3.2 \times 10^5$) is used as the transition criterion for this oscillating case, the boundary layer is laminar for all conditions investigated. Assuming that the boundary layer thickness formula, $\Delta = 5x/\sqrt{Rx}$, which is derived for constant velocity flow over a flat plate (x is the distance along the plate), is applicable to the oscillating flow case, the calculated boundary layer thicknesses are shown at the respective Reynolds numbers in Figure 16. From these it is seen that only the largest grit size protruded beyond the boundary layer at the maximum velocity part of the cycle. At the two lower Reynolds number test conditions, all of the grit sizes were submerged in the laminar boundary layer. (Figure 17 shows the logarithm of the amplitude versus cycle for several test conditions. The slope of these lines is constant, indicating that δ = log decrement is

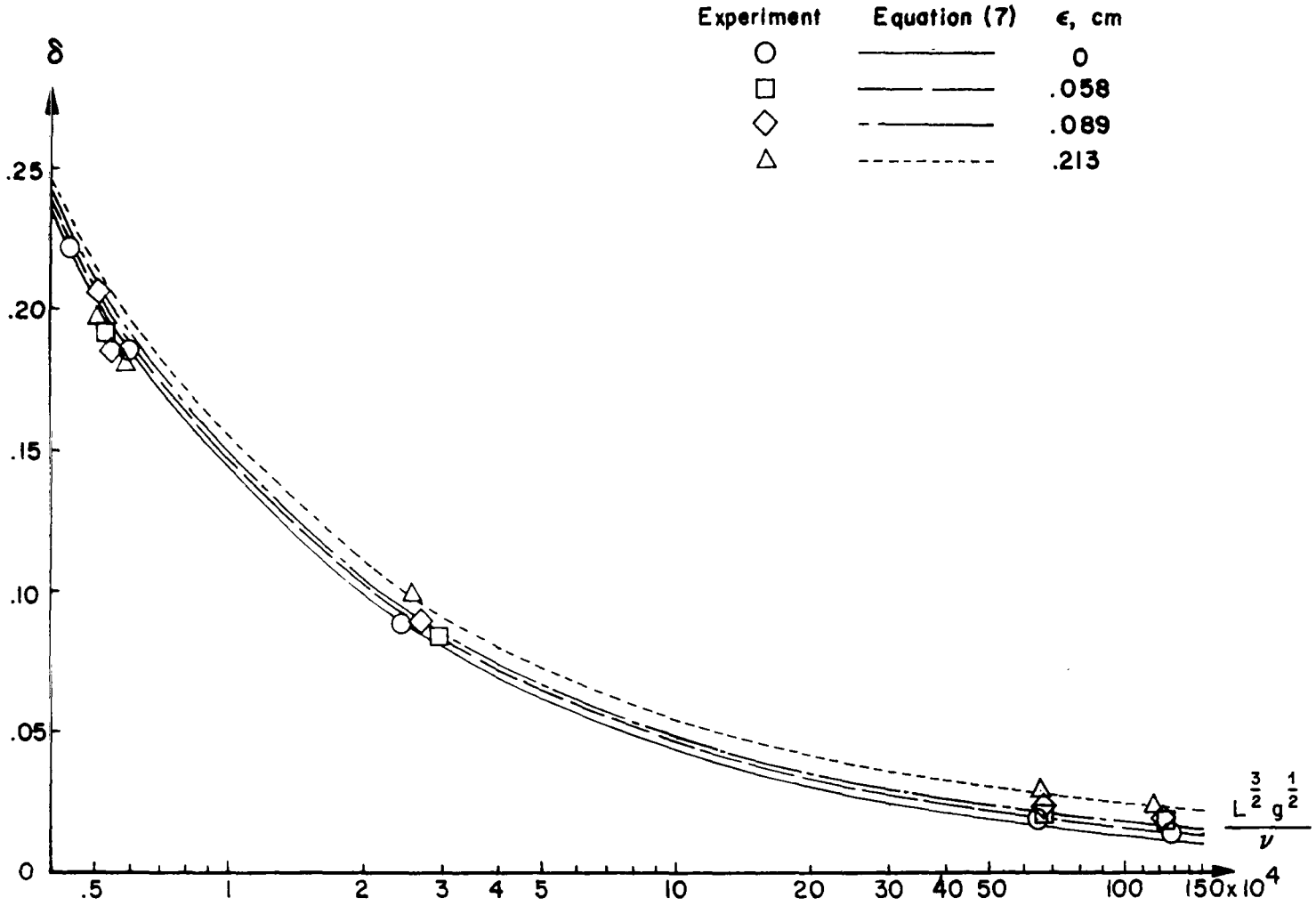

Figure 15. Curve fit of data by empirical formula.

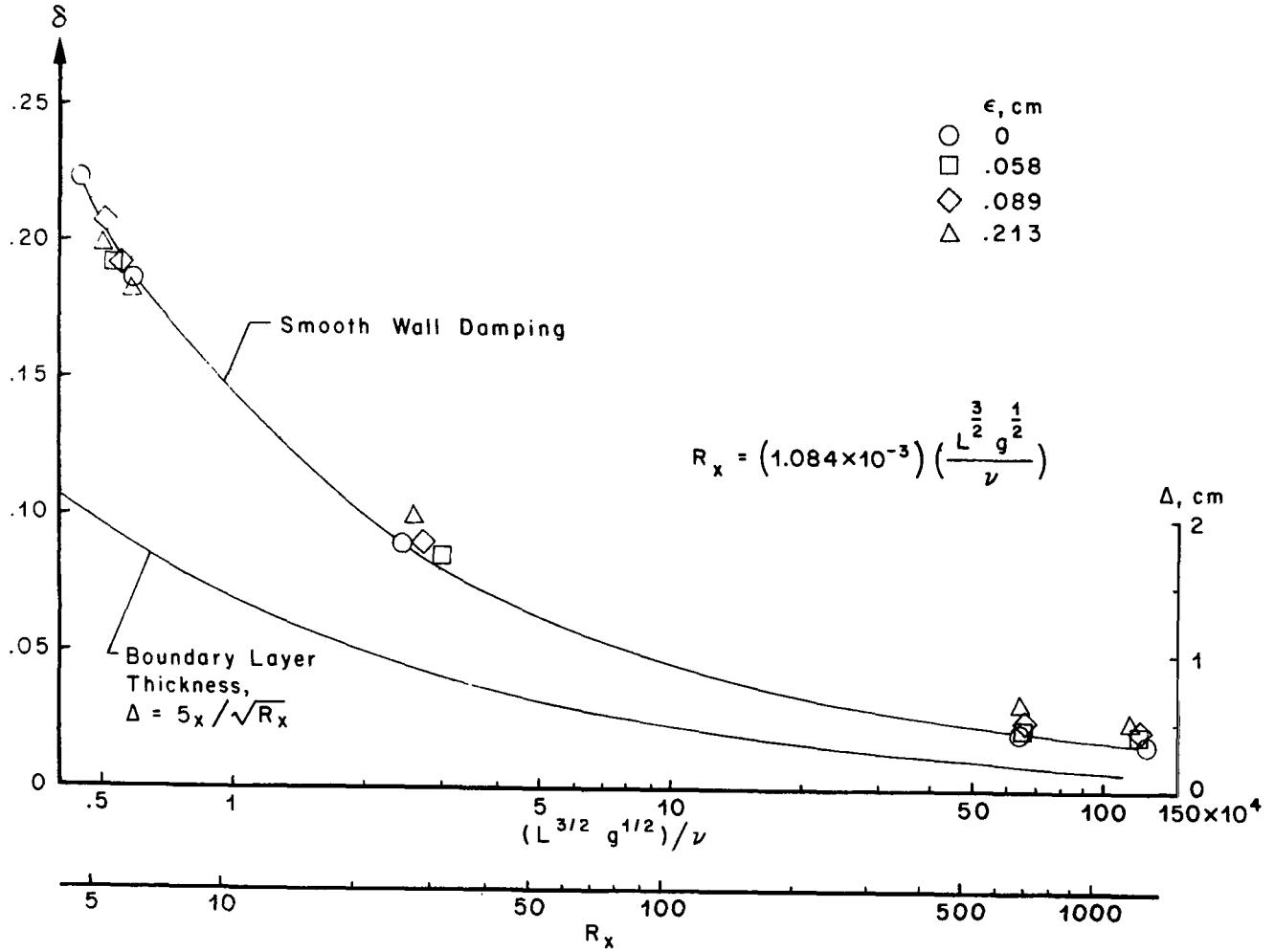

Figure 16. Reynolds number and boundary layer thickness.

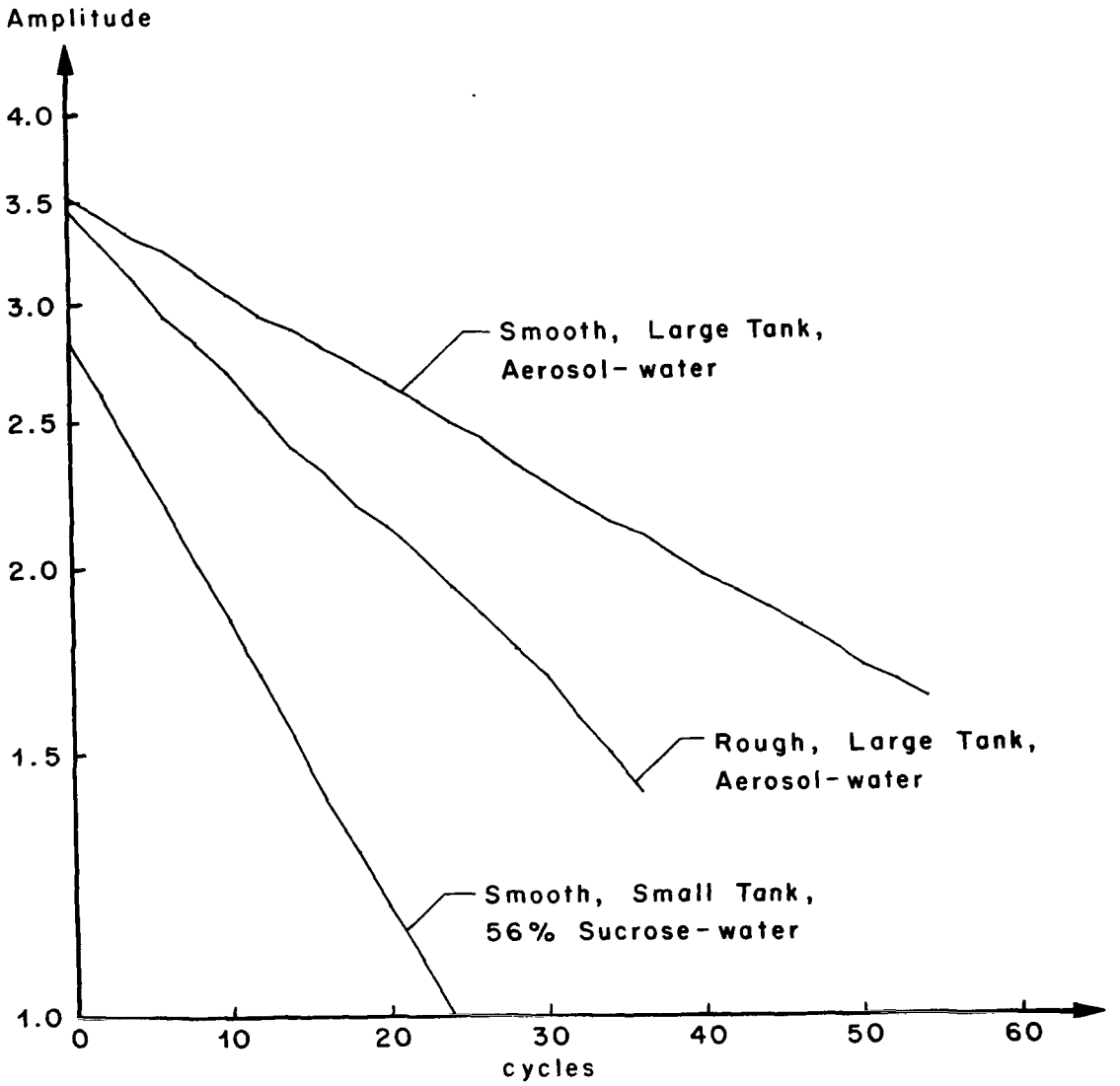

Figure 17. Amplitude decay.

constant, independent of amplitude in this range of amplitudes. For a particular decay one value of δ will result, but the value of Rx as previously defined will vary with the square of the starting amplitude of decay.)

If the grit particles are submerged in the boundary layer during a significant portion of each cycle, then the mechanism of damping by wall

roughness is not primarily the increase of viscous damping at the wall. If wall roughness does not increase the viscous damping, then the damping because of wall roughness should be independent of $L^{3/2}g^{1/2}/\nu$, the parameter on which viscous damping depends. (The data show that the damping because of roughness is independent of $L^{3/2}g^{1/2}/\nu$.)

If the contact angle changes during the liquid oscillations, then surface tension can provide damping. The wetted perimeter at the tank ends was computed from the dimensions of the various grit sizes and divided by twice the tank width; it was then plotted against δ to form Figure 18. If the main effect of roughness is to increase the wetted wall perimeter for the surface tension to work on, then the loss of effectiveness at the low Reynolds number is logical since the high viscosity test liquid filled the spaces between roughness particles, reducing the wetted perimeter to near the smooth-wall perimeter, and remained during the decay.

Some calculations indicate that the change in damping measured from smooth to rough wall in the small tank with the low viscosity could result from surface tension effects if the contact angle changed from 0 to 29 degrees during each oscillation. From the literature the variation of contact angle of a drop of mercury on a flat glass plate with plate inclination is 27 degrees. The contact angle hysteresis of water on paraffin was 16 degrees.

CONCLUDING REMARKS

An experimental investigation was made to determine the effectiveness of wall roughness for damping liquid oscillations in rectangular tanks. The following results were obtained.

1. The value of log decrement of damping, δ, increased in a nearly linear fashion as the roughness height was increased. With roughness of which the height was 0.427 percent of the tank length covering 8.9 percent of the wetted wall area δ was 65 percent greater than the smooth-wall value.

2. Roughness near the liquid surface was more effective in damping liquid oscillations than roughness deep in the tank. There was a sharp increase in damping corresponding to wiping of the roughness by the surface edge during decay. Maximum damping was produced by a particular roughness strip when the strip was at the maximum depth at which the surface edge wiped the roughness throughout decay of the oscillation. Narrow strips

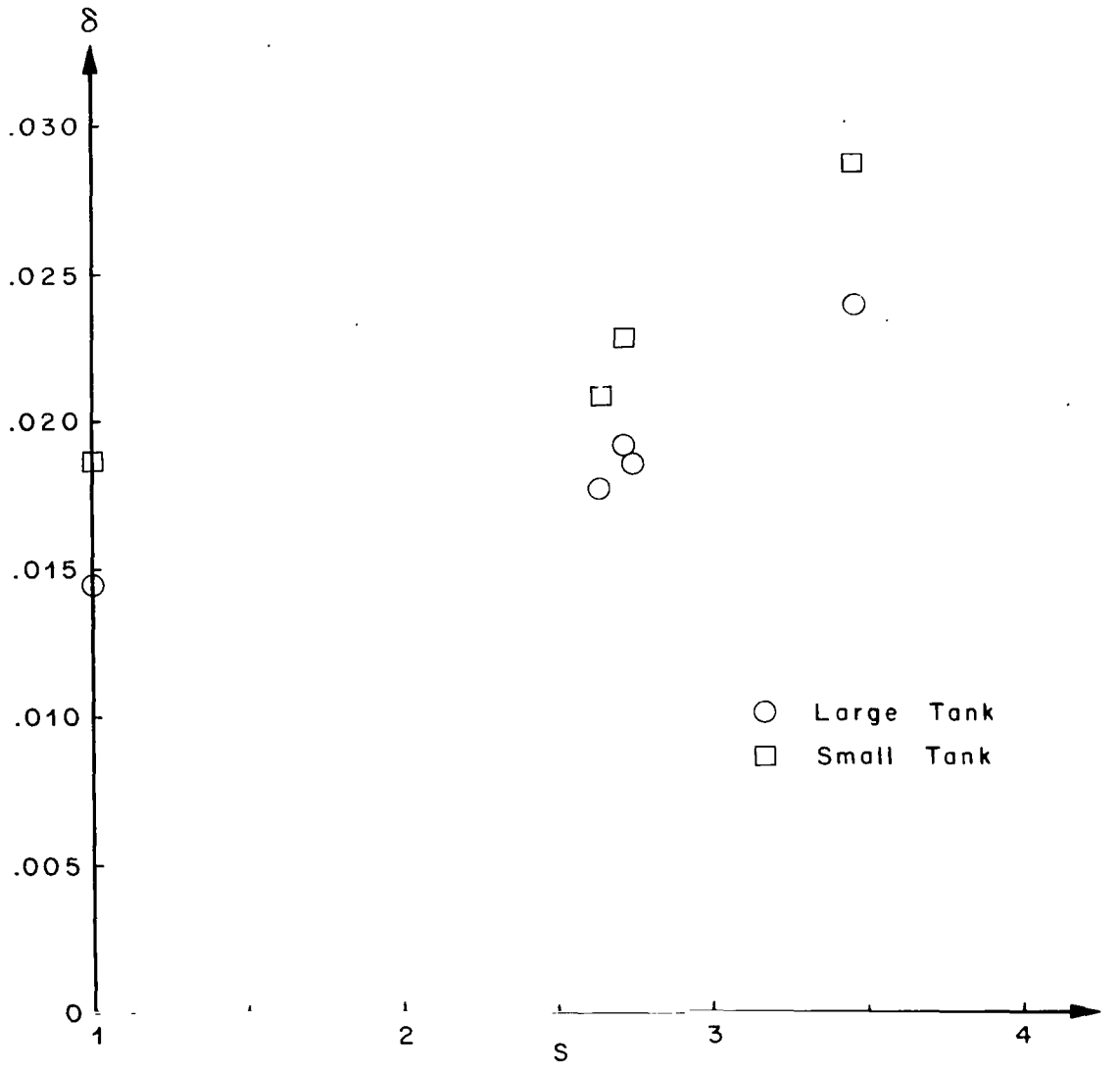

Figure 18. Effect of wetted perimeter on damping.

of roughness (3.6 percent of the wetted wall area) in contact with the liquid surface edge during decay were found to produce 75 percent as much damping as roughness covering the entire end walls of the tank (36 percent of the wetted wall area).

3. The damping was found to increase with decreasing values of $L^{3/2}g^{1/2}/\nu$, but the increment of damping because of wall roughness remained nearly constant through most of the $L^{3/2}g^{1/2}/\nu$ range. The increment of δ because of a particular wall roughness configuration was 34.5 percent of the total δ at $L^{3/2}g^{1/2}/\nu = 650\ 000$ and was only 13.5 percent of the total δ at $L^{3/2}g^{1/2}/\nu = 27\ 000$.

4. A formula was constructed to fit the smooth-wall damping data through the range of values of $L^{3/2}g^{1/2}/\nu$ investigated by multiplying Keulegan's equation for smooth-wall damping [13] by an empirical constant. An expression formed by adding a term dependent on roughness height relative to tank length to the above formula gave a fair representation of the effect of roughness height on damping through a range of $L^{3/2}g^{1/2}/\nu$ values for a particular roughness configuration.

5. Reynolds number and boundary layer thickness calculations indicated that the test roughness should have little effect on viscous damping. Other calculations showed that the damping because of roughness could be produced by surface tension acting on the roughness-height-dependent wetted perimeter through a changing contact angle.

George C. Marshall Space Flight Center
National Aeronautics and Space Administration
Marshall Space Flight Center, Alabama, 35812, October 24, 1969
933-50-00-00-62

REFERENCES

1. Bauer, H. F.: Fluid Oscillations in the Containers of a Space Vehicle and Their Influence Upon Stability. NASA TR R-187, February 1964.

2. Buchanan, H. J.; and Bugg, F. M.: Orbital Investigation of Propellant Dynamics in a Large Rocket Booster. NASA TN D-3968, May 1967.

3. Masica, W. J.: Experimental Investigation of Liquid Surface Motion in Response to Lateral Acceleration During Weightlessness. NASA TN D-4066, July 1967.

4. Brady, W. F.; Pope, M. D.; and Pode, L.: Ablestar Experimental Sloshing Studies. Report No. SGC 32R-19, Contract No. AF04 (647)-621 and AF04(695)-17, Space General Corporation, August 1962.

5. Garza, L. R.; and Abramson, H. N.: Measurements of Liquid Damping Provided by Ring Baffles in Cylindrical Tanks. Technical Report No. 5, Contract No. NAS8-1555, Southwest Research Institute, April 1963.

6. Stricklin, G. P.; and Baird, J. A.: A Survey of Ring Baffles Damping in Cylindrical Tanks, Technical Note R-185, Contract No. NAS8-20073, Brown Engineering Company, Inc., April 1966.

7. Mikishev, G. N.; and Doroshkin, N. Ya.: An Experimental Investigation of Free Oscillations of a Liquid in Containers (in Russian). Izv. Akad, Nauk SSR, Dtd. Tekh. Nauk, Mekh. i Mashinostr, No. 4, July/August 1961, pp. 48-83. Transl. into English by D. Kana, Southwest Research Institute, June 30, 1963.

8. Dodge, F. T.; and Garza, L. R.: Experimental and Theoretical Studies of Liquid Sloshing at Simulated Low Gravities. Technical Report No. 2, Contract NAS8-20290, Southwest Research Institute, October 1966.

9. Abramson, H. N.; and Ransleben, Jr., G. E.: Simulation of Fuel Sloshing Characteristics in Missile Tanks by Use of Small Models. Technical Report No. 7, Contract No. DA-23-072-ORD-1251, Southwest Research Institute, April 1960.

REFERENCES (Concluded)

10. Garza, L. R.: A Comparison of Flexible and Rigid Ring Baffles for Slosh Suppression. Technical Report No. 1, Contract No. NAS8-20290, Southwest Research Institute, August 1966.

11. Case, K. M.; and Parkinson, W. C.: Damping of Surface Waves in an Incompressible Liquid. Journal of Fluid Mechanics, vol. 2, 1957.

12. Berlot, R. R.; Birkhoff, G.; and Miles, J. W.: Slosh Damping in a Rigid Cylindrical Tank. Report No. GM-TR-263, Ramo-Woolridge Corporation, October 1957.

13. Keulegan, G. H.: Energy Dissipation in Standing Waves in Rectangular Basins. Journal of Fluid Mechanics, vol. 6, July 1959, pp. 33-50.

14. Handbook of Chemistry and Physics. Chemical Rubber Publishing Company (Cleveland), 1963.

NASA-Langley, 1970 — 12 M159